Semi-empirical 2D model of the solar corona and solar wind using solar eclipse images: Progress report

Edward C. Sittler Jr.[ID] and Linda M. Sittler

email: edwardsittler@gmail.com

Abstract. We present white light images of the Sun's corona acquired during the total Solar Eclipses on August 21, 2017 in mountains north of Boise Idaho USA and on July 2, 2019 south of Copiapo Chile. In both cases the viewing was excellent, altitudes ~ 1200 m and relative humidity $\sim 10\%$. We used an Orion equatorial reflecting telescope with 203 mm diameter aperture and 1000 mm focal length for f4.9 optics. A computer-controlled Canon EOS Rebel T3i digital camera was used. We plan to use our 2019 eclipse images for analysis since the Sun is near solar minimum so 2D steady state MHD equations can be used. We present a plan to process the images and convert them into a 2D empirical model of electron density and magnetic field in radial distance and co-latitude, from which 2D maps of flow velocity, effective temperature and effective heat flux can be computed.

1. Introduction

As discussed in Habbal *et al.* (2011) eclipse observations provide unique information about the solar corona just above the limb from the solar surface out to a few solar radii where the thermodynamic and magnetic properties of the coronal plasma is most complex, usually not provided by coronagraphs in space, and is a region of most importance where the expansion of the solar magnetic field and solar wind acceleration is occurring. This inner most region 3D MHD models have the most difficulty and the underlying physics is not well understood. One can model the photospheric magnetic field quite well below the corona and at higher altitudes where the flow is supersonic beyond the sonic critical point. But this region of transition cannot be modeled well theoretically, so a semi-empirical approach as first attempted by Sittler & Guhathakurta (1999, 2002) or SG model was performed using satellite and ground-based coronagraph data. Here we note in a recent paper by Woo (2019) who discusses past solar eclipse images, including the August 21, 2017 solar eclipse, some using photographic film, others based on drawings using naked eye observations and those more recently using cameras with CCD detectors and what can be learned from the various solar eclipse images. In this paper we will be just presenting the observations made for the August 21, 2017 solar eclipse in the state of Idaho and the July 2, 2019 solar eclipse south of Copiapo Chile. Regarding the analysis of the observations we will outline our approach to processing the data which is still in progress and not ready for this report. We will then present the 2D semi-empirical model we used in the Sittler & Guhathakurta (1999, 2002) papers and will mention how it could be generalized to 3D, which when combined with 3D MHD models that include the continuity, momentum and energy equations, could provide the quickest path to modeling the coronal expansion and further our understanding of the solar corona's heating, acceleration and energy transport.

Figure 1. Shows telescope used during the August 21, 2017 solar eclipse up in the mountains north of Boise Idaho at an altitude 1219 m. One can see the clear blue skies for the eclipse observations. See text and Tables 1-3 for details.

2. Telescope Description

In Figure 1 we show the telescope as used for the August 21, 2017 solar eclipse in the mountains north of Boise Idaho. The figure shows the Orion Equatorial Reflecting Telescope with 203 mm diameter aperture with focal length of 1 m for f4.9 optics, secondary mirror with 58 mm minor axis, SkyView Pro, German equatorial mount, steel tripod, and RA/Dec motor drives controlled by Orion SynScan V5 GoTo Hand Controller. The telescope mount weighs 30 lbs, optical tube 32 lbs and the two counterweights weigh 10.9 lbs each. Orion Solar Glass Filter with $\sim 100{,}000$ light rejection can be seen covering the telescopes aperture, and a computer-controlled Canon EOS Rebel T3i single reflex camera with 5184 x 3456 pixels (17.9 MP, 50 mm OD) CCD mounted where telescopes eye piece would normally be located. The camera can be manually moved up/down for focusing. With filter on during partial eclipse periods we used shutter speed 1/30 s for 2017 solar eclipse, therefore over-exposed, while for 2019 solar eclipse we used 1/2000 s shutter speed, images not over-exposed. USB serial interface cable from Dell Inspiron 13 laptop computer goes to metal converter box (i.e., acts as switch for shutter, circuit used came from website by Paul Beskeen 2009) which can be seen with its output red cable going to the camera's shutter control terminal which triggers when the shutter opens so images spaced ~ 1 s can be achieved. The other USB serial cable from the computer goes to the camera's digital control terminal so one can configure camera settings to ISO 100, set shutter speed, store raw images and have images stored directly to the cameras memory card so images ~ 1 s apart can be taken (i.e., speed to transfer images to the computer takes too much time). Batteries not shown were used to provide power for the equatorial mount motors, and laptop computer (not so for July 2, 2019 but computer battery lasted well after total eclipse). The camera has its own lithium batteries which were replaced just before total solar eclipse as was done for the camera's memory card. We also fine-tuned the focusing by eye using the computer screen just before total eclipse. For both eclipses the tracking was not perfect. For the 2017 and 2019 total eclipses we used two shutter times of 0.3 s and 1/30 s, and three shutter times of 0.3 s, 1/30 s and

Table 1. Canon EOS Rebel T3i Camera Parameters

Parameter	Eclipse 08/21/2017	Eclipse 07/02/2019
ISO	100	100
Shutter Trigger	External via USB	External via USB
Image	Raw	Raw
Pause	500 ms	0 ms
Store Images	Camera Memory Card	Camera Memory Card
Shutter Speed ΔT	0.3 s, 1/30 s, 1/30 s	0.3 s, 1/30 s, 1/500 s

1/500 s, respectively. In order to control the camera we used a software package called Astro Photography Tool (APT) "Eclipse Beta v3.36" (v3.36 was a delta version made by the providers for the 2017 solar eclipse so images could be recorded quickly; normally for astrophotography they usually integrate for long periods of time for good signal to noise S/N measurements). Using this method, we recorded excellent images of the Sun's corona.

3. Observational Method Used

The use of the wide aperture reflecting telescope was to achieve the highest spatial resolution allowed by atmospheric effects and to image the polar corona with altitude out beyond one solar radius. Near the Sun the E-corona from electrons should dominate the F-corona from interplanetary dust so polarized light observations would not be required. The 2019 eclipse occurred near solar minimum and as the images show the corona displays a single equatorial streamer belt which is expected when at solar minimum. We used a computer-controlled camera so one could take images as quickly as possible since for the two total eclipses used here lasted only about 1-2 minutes. The providers of the APT software v3.36 allows one to reduce the delay between images ≤ 500 ms and have control of the shutter via a different USB serial port rather through the camera itself which evidently is much slower. For the 2017 eclipse we set the APT pause (i.e., delay) parameter equal to 500 ms for delay between images, while for 2019 eclipse we used no delay. With v3.36 one can run up to 20 images for a sequence which take ~ 1.7 s per image or ~ 34.29 s and then restarted almost immediately by the operator when that sequence ends. For the 2017 eclipse we recorded $\sim$64 images when total, while for the 2019 eclipse we recorded ~ 60 images when total. For both eclipses we had three shutter speeds (in case of 2017 eclipse two were identical at 1/30 s) so there were 21 sets of images with the 3 shutter speeds for each set for 2017 eclipse and 20 sets for the 2019 eclipse. Empirically, using the APT clock, we estimated the 2017 eclipse began on August 21, 2017 at 1:26:04 and ended at 1:28:32 for 2017 (i.e., 2 min 28 s long), while for the 2019 the start and stop times were July 2, 2019 04:39:15 and 04:40:57 (i.e., 1 min 42 s long), respectively. In Tables 1, 2 and 3 we list all relevant parameters for the two eclipses, respectively.

For both solar eclipses we arrived at the observation sites several hours before the partial eclipse phase would begin. For the 2017 eclipse we were north of Boise Idaho in the mountains at elevation ~ 1219 m and not a cloud in the sky. Using the National Geophysical Data Center, we recorded the coordinates of the Sun/Moon at the time of the eclipse RA ~ 10 hr 4 min and declination 11° 52 min and its magnetic declination for our location $\sim 13.5^o$ E. We then setup the telescope with tripod north equatorial axis point to the north magnetic pole using a compass, string and nails on each end and nailed to the ground. We then aligned the tripod using plumb bob, so its central axis intersected the string. We then put another string from the other two legs, so it crossed the magnetic axis string at 90°. This was achieved when the distance of the two legs and the magnetic axis string were the same. In addition, we used a circular level, so tripod was level with respect to the local ground. Around this axis we rotated the tripod by

Table 2. Orion Reflecting Telescope Parameters

Aperture	203 mm
Focal Length	1000 mm
Focal Ratio	F4.9
Shadow Parameter	0.92
2nd Mirror Focal Length	58 mm
Mount	SkyView Pro, German Equatorial
RA/Dec	Motorized Hand Controller
Focusing	Manual
Tripod	Steel
Orion Solar Filter Transmission	10^{-5}
Compass	Align tripod with magnetic north or south
360° Level	Level Telescope with local ground
Plumb Bob	Used to align tripod with geographic poles
Telescope Weight	62 lbs
Counterweights Weight	10.9 lbs each

Table 3. Solar Eclipse Site

Eclipse	Altitude	Sun RA	Sun Dec	Mag Dec	LMT[1]	Start[1,2]	Stop[1,2]
21/08/17	1219 m	10 h 4 m	11° 52 m	13.5°E	12:47:49	1:26:04[3]	1:28:32[3]
02/07/19	1200 m	6 h 46 m	23° 0 m	2.25°W	12:44:15	4:39:15[2]	4:40:57[2]

[1]LT is given.

[2]In July Chile LT is same as EDT which is -4 hours relative to GMT.

[3]In August Boise Idaho LT is -6 hours relative to GMT.

13.5^o W so it was now aligned with the Earth's geographic spin axis. Then the telescope was mounted with counter balancing weights installed, solar filter installed and then rechecked with level to make sure tripod still level. We then installed the camera with its view finder on so we could see the Sun once properly aligned. We also had to correct for precise time when Sun would intersect the local meridian which would then give the RA/Dec of the local meridian at that time since we knew the RA/Dec of the Sun. This was important since the field-of-view (FOV) of the telescope was only $\sim 1^o$ x 1°. We then tried to find the Sun and failed for the first attempt, we then realized a mistake was made and once repeated we found the Sun nearly immediately. In the case of the 2019 eclipse the magnetic declination was $\sim 2.2^o$ W so we did not attempt to make this correction. For the 2019 eclipse we did not realize the secondary mirror was miss-aligned during shipping with its four-vaned spider holder (i.e., vanes only 0.4 mm thick) were badly twisted out of shape. Fortunately, we were able to get the vanes straightened out properly and using the manual with allen wrench to make the needed fine adjustments, so the secondary mirror was approximately aligned (note, Dr. Christian Hummel helped us fix this unexpected problem). Within minutes we found the Sun and then using the equatorial motors put the telescope into solar tracking. Since the alignment was not perfect every so often, we would have to use the hand motor controller to put image back into the center of the camera FOV. During total eclipse this was not needed. Once solar tracking achieved, we completed the connections of the camera with the laptop computer and the metal converter box for the shutter control. Now the image would appear in the APT viewing window. Then as described above, we used the APT software to control the camera during both partial and total eclipse phases. During partial eclipse the images were spaced about 5 s apart. Just before total we put APT software into the total eclipse mode and based on the darkening as we approach total, we removed the solar filter and similar but reverse approach was used when total eclipse was ending. While in total eclipse mode the images were going to the camera memory card and one cannot see the
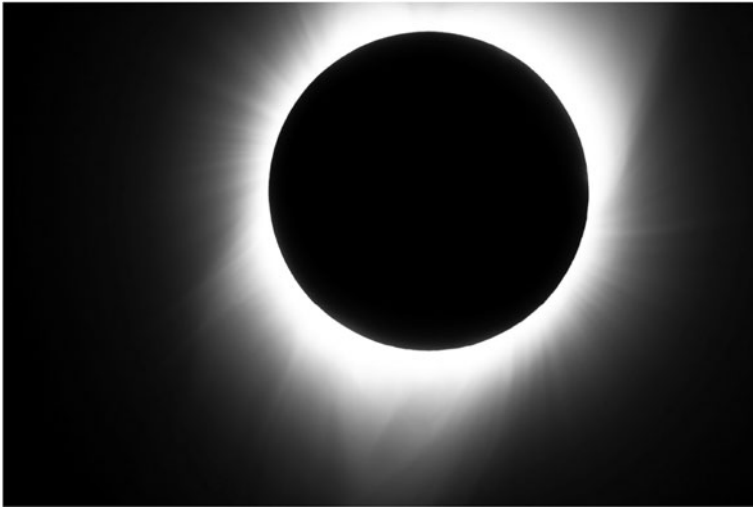
Figure 2. August 21, 2017 total solar eclipse image 7799 with 1/30 s shutter speed used. At this time the Sun is in transition from solar max to solar min so reason for several overlapping equatorial and mid-latitude streamers. With a few tenths of solar radius altitude, the equatorial streamers are over exposed, while the polar streamers are not except very near the lunar edge.
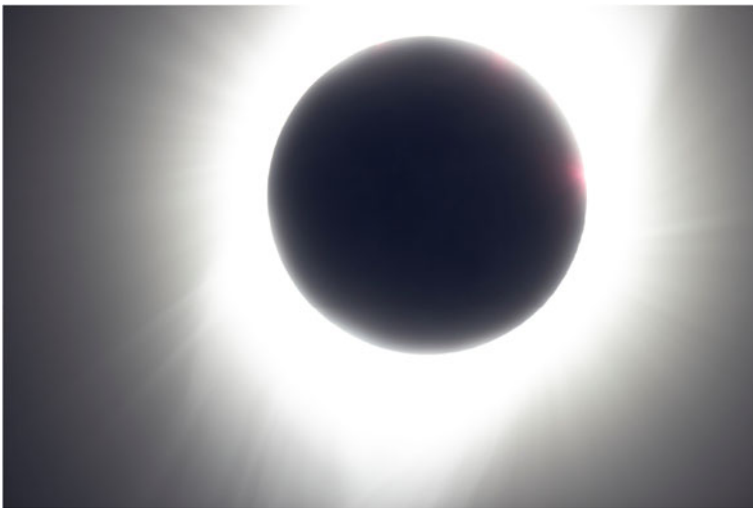

Figure 3. August 21, 2017 total solar eclipse image 7800 with 0.3 s shutter speed used. Near the Sun most of the image is over exposed as expected but when combined with image 7799 in Fig. 2 can allow extension of the observations to the outer boundaries of the image FOV.

Sun's image until after total. By inspecting images later some were over exposed but got it approximately right. Note, some of the details were recorded and some were based on memory.

4. Results: August 21, 2017 Solar Eclipse

We show in Figures 2 and 3 representative images of the solar corona taken during the 2017 solar eclipse using the telescope shown in Figure 1. These images are what some refer to as thumb nail low resolution images of the raw images which are ~ 17.9 MP in size with each pixel 16 bits deep (note, not all 16 bits are usable). We have made preliminary

Figure 4. Diamond ring effect in this image 7824 taken just after the August 21, 2017 total eclipse ended and shows that the moon is moving along a line 45° from top right to lower left which is approximately where the ecliptic plane is located.

processed images using the raw images of those shown in Figure 2. One can combine these two images most simply by just renormalizing say image 7799 by the ratio 0.3∗ 30 = 9 and then adding the two images with regions of over-exposer removed. As discussed below the processing will be more complex. Using the raw images 5184 x 3456 pixels the Sun/moon are ∼ 2195 pixels in diameter and since 0.5^o wide in the sky, each pixel is ∼ 0.5 degrees x 3600 arcsec/degree / 2195 pixels ∼ 0.8 arcsec/pixel. When looking at the images under high magnification they became blurred, so the actual spatial resolution was likely several arcsec to be determined. Since the Sun is in transition from solar max to solar min the equatorial region is more complex and composed of multiple streamers and within a few tenths of solar radius above the limb the image in Figure 2 is over exposed (1/30 s exposure time). In the polar regions where polar plumes can be seen and evidently showing the dipolar curved nature of the Sun's polar magnetic field the images are not over exposed except very close to the limb this may occur. Note, these are inverted images and we note the moon's motion is tilted ∼ 45° in the image with the moon moving from upper right to lower left which is shown by Figure 4 from image 7824 which shows diamond ring effect near end of the solar eclipse. In Figure 3 out to a few tenths of a solar radius even the polar regions, as expected, are over-exposed. For our semi-empirical modeling which is presently 2D we will not use the 2017 images except for the polar corona.

5. Results: July 2, 2019 Solar Eclipse

Like the 2017 solar eclipse, we here show in Figures 5, 6 and 7 representative images of the solar corona taken during the July 2, 2019 solar eclipse using the same telescope shown in Figure 1 for the 2017 eclipse. The main difference is now we also have images with 1/500 s shutter time intervals which allows us to have good images all the way down to the solar limb. This is shown in Figure 5 and since inverted images and moon slightly offset to the north, one can see evidence of the chromosphere within the south polar region. This figure also shows evidence of active region arches on both sides near the south polar boundary and likely extends all around the Sun. These coronal arches are ∼ 45° from vertical and the symmetry axis of these arches appear to be slightly tilted

Figure 5. July 2, 2019 solar eclipse image taken south of Copiapo Chile using the telescope, camera and computer described in the text. This image is a highly compressed pdf version of raw images 18 MB in size. Shutter time 1/500 s.

Figure 6. The same as in Figure 5 for shutter time 1/30 s.

in counterclockwise direction opposite of what appears to be the case when looking at the polar plumes in Figure 6 (i.e., indicates slight tilt in clockwise direction). We do not see similar coronal arches to the north or bottom of figure for which the moon is slightly tilted to the north and thus covering more of the solar limb. For this eclipse, as shown in Figure 8 for image 9744 near beginning of the 2019 total solar eclipse, the moon is moving from lower right to upper left at angle $\sim 45^o$. Again, as for the 2017 eclipse these images are thumb nail low resolution versions of the raw images which are ~ 17.9 MP in size. We have not yet made preliminary processed images of the raw images for this eclipse. In this case one can combine all three images weighting 5 by $500/30 \sim 16.67$, replace those pixels in Figure 6 that maybe over-exposed with those in Figure 5, and reduce the amplitude of those in Figure 7 by 1/9. One can then renormalize so min count
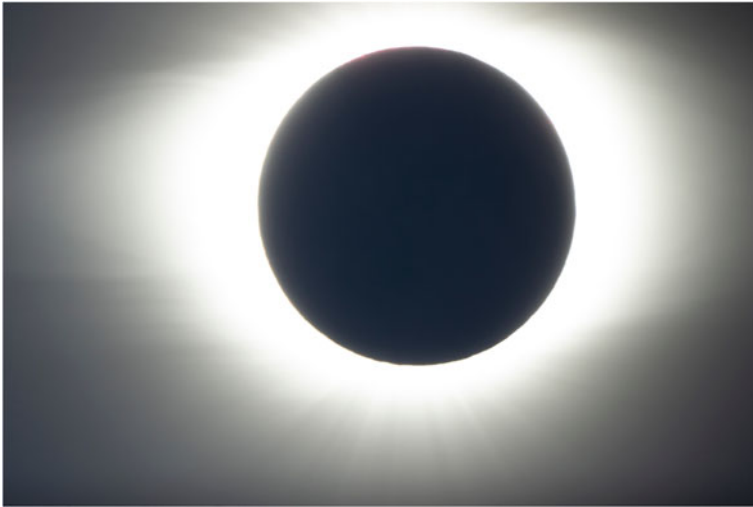
Figure 7. The same as in Figure 5 for shutter time 0.3 s.

Figure 8. Diamond ring effect in this image taken just before total eclipse for the July 2, 2019 solar eclipse. This image indicates the moon is moving from lower right to upper left in the image. Figures 5-7 indicate the equatorial streamers are from left to right so the polar regions will be nearly vertical in the figure.

is ~ 1 at the outer boundaries of the images. Again, the processing discussed below will be more complex. For this eclipse the Sun is near solar min and as expected only a single equatorial streamer is evident in the images so will work best with our 2D semi-empirical model of the solar corona and solar wind.

6. Planned Data Analysis Method

6.1. Processing of Images

When it comes to processing of raw images there is good article on the internet by Sumner (2014) which describes raw sensor data structure, and how to incorporate the raw Canon CR2 images into MATLAB. The CR2 files contain uncompressed image containing

pixel values plus meta-information or header information about the image referred to as tags. The first step is to convert the images into Digital Negative or DNG files using an Adobe DNG Converter. The DNG files are similar to TIFF files. Within the MATLAB environment one can perform a series of operations such as Linearization, White Balance, Demosaicing, Color Space Correction and Brightness and Contrast Control. All these steps are used to make good quality images for display purposes on one's computer monitor but for scientific purposes some we may not use, but all can be done in MATLAB. We have performed some of these steps to our 2017 images with some success for display purposes.

In order to process these images, one must perform several steps which includes the calibration of our camera + telescope as discussed in article by Clark (2013). This will involve the observation of the 0-magnitude star Alpha Lyra (RA 18h 36m 56s & Dec $+38^o$ 47' 1") as our candle (see Schild *et al.* 1971) and using filters at specific wavelengths. One can then take these measurements and compare with known intensities for Alpha Lyra $\sim 10^{11}$ photons/m^2/s/micron, then using green filter at 0.53 microns, with its FWHM $\sim$0.077 in microns, $\sim 7.7 \times 10^9$ photons/m^2/s will pass through the filter, then correcting for atmospheric transmission for clear atmosphere $\sim 85\%$ to give $\sim 6.5 \times 10^9$ photons/m^2/s near sea level. From the recorded data at known shutter exposure times, camera at ISO 100, aperture of telescope 203 mm diameter, shadow effect for telescope, and CCD counts in DN (integer Data Numbers) and typical camera 12-bit DNs are mapped into the same scale as the computer 16-bit DNs one can then estimate the number of photons/DN for the camera. In the case of the Sun we used a solar filter with transmission $\sim 10^{-5}$, while for Alpha Lyra it will be ~ 1. In the example given by Clark, 2013 the Canon camera 10D digital camera it was estimated ~ 28 photons/DN at ISO 400. In our case the lens elements are removed. Other parameters are fill factors $\sim 25\%$ to 80%, typical quantum efficiency range between 19% to 26%, green filter transmission $\sim 90\%$, and if needed how to convert lux into photon intensities when comparing different stellar sources. The Sun is $\sim 4 \times 10^{10}$ more intense than Alpha Lyra. In the case of Alpha Lyra only a few nearby pixels will receive signal from the star while in case of the Sun ~ 15 MP (occulted part of image by moon ~ 3 MP not counted) will be *illuminated*, so will need to scan the star across the CCD since the response may not be uniform and not sure how the response may have been effected when over-exposed. I would expect the performance of our Canon EOS Rebel T3i to be better than the Canon 10D camera used in Clark's observations back in 2013. In addition, our calculations of the data should be close to the typical intensities of the Sun.

6.2. *Combine Images*

It may also be necessary to combine images as discussed in the paper by Druckmüller (2009) (also see Reddy & Chatterji 1996) who developed a modified phase correlation method based on Fourier transforms which enables alignment of coronal images taken during solar eclipses, and can measure translation, rotation and scaling factors between images. This will be very important for our measurements for which the alignment was clearly not perfect. Even though the tracking needed manual updates this was not done during the total eclipse phase which was $<$ a few minutes. Once the above is done we would be able to convert the images into electron density radial and latitudinal profiles.

6.3. *Convert Images to 2D Electron Density Maps*

The conversion of the images into electron densities would follow the approach described in Guhathakurta *et al.* (1996) and references within such as the classic paper by Hulst & van de (1950) and the review article about the interpretation of total eclipse

images in the early days by Hulst & van de (1953). In our case we expect our images to be dominated by the K-corona due to Thompson scattering of light by free electrons. The F-corona is more important further out radially, but we will investigate its importance for the eclipse in 2019. The Guhathakurta *et al.* (1996) results were based on polarized brightness pB data from *Skylab* HAO white-light coronagraph (WLC) images and ground based K-coronameter images of the corona (i.e., High Altitude Observatory (HAO) Mark II K-coronameter at Mauna Loa (1.12 to 2.0 R_{SUN}) and the HAO coronal eclipse camera). One would expect such ground-based coronagraphs would be taking images of the corona during both eclipses and provide information of the K-corona and F-corona so corrections could be made if necessary.

7. Electron Density Model

We will then use the electron density model developed by Sittler & Guhathakurta (1999, 2002) and fit it to our derived electron density profiles. The model used is briefly:

$$N(r, \theta) = N_P(r) + [N_{cs}(r) - N_P(r)] e^{-\lambda^2/w^2(r)} \tag{7.1}$$

for which latitude $\lambda = \pi/2 - \theta$ and θ is the colatitude. $N_P = a_{P1} e^{a_{P2}z} z^2 P_P(z)$ and $P_P(z) = 1 + a_{P3}z + a_{P4}z^2 + a_{P5}z^3$ with a_n as free parameters to be fit to the data. The subscript P stands for polar regions and CS the current sheet region and z = R_{Sun}/r. The variable w(r) gives the radial variation of the equatorial helmet streamer angular width which increases with r. A similar set of equations apply for $N_{CS}(r)$. Then using Eqs. 21-23 in Sittler & Guhathakurta (1999) we solve for the field line equation and by using the lower boundary of the polar coronal hole we fit the parameters for monopole $\eta_M = 2B_M/B_0$, dipole $\eta_D = B_D/B_0$ and quadrupole $\eta_Q = B_Q/B_0$ terms. The magnetic constant B_0 is set by the radial component of the magnetic field which is ~ 3 nT at one astronomical unit or AU from the Sun. We could also use the radial component of the magnetic field measured by the Parker Solar Probe spacecraft. Once B_0 is known one can then estimate the magnetic field strength at the base of the corona and can be compared with corresponding values based on solar magnetogram observations. Once available we will also use electron density measurements made by the Parker Solar Probe instruments to get a better constraint on the equatorial radial profiles. The same can be said for the radial magnetic field measurements.

8. Theoretical Description

8.1. *Mass, Momentum and Energy Equations*

We plan to convert our empirical electron density radial and latitudinal profiles into 2D maps of solar wind velocity, effective temperature and effective heat flux using the method and equations described in the Sittler & Guhathakurta (1999, 2002). Starting from the basic MHD equations of the coronal expansion in steady state one can then transform the equations into the rotating frame of the Sun which allows one to include the Parker spiral pattern of the interplanetary magnetic field in the solution and solve for various field line constants. One then ends up with the following equations:

$$\rho \vec{V} = \alpha \vec{B} \tag{8.1}$$

$$T_{eff} = \frac{\mu m_H}{\kappa} \left(\frac{1}{\rho} \int_l^\infty W' \frac{d\rho}{ds} ds \right) \tag{8.2}$$

$$W' = \frac{1}{2} \left(V_P^2 \infty - V_P^2 \right) + \frac{1}{2} \left(\Omega^2 R^2 - \frac{\alpha^2 B_t^2}{\rho^2} \right) + \frac{1}{2} v_{esc}^2 z \tag{8.3}$$

$$v_{esc}^2 = \frac{2GM_{Sun}}{R_{Sun}} \quad \text{and} \quad z = R_{Sun}/r \tag{8.4}$$

$$q_{eff} = \rho V \left(W' - \frac{5}{2} \frac{P_{eff}}{\rho} \right) \tag{8.5}$$

$$P_{eff} = \rho \kappa T_{eff}/\mu m_H \tag{8.6}$$

for which μ is mean molecular weight with 5% helium abundance assumed, m_H is proton mass, κ is Boltzmann constant, G is gravitational constant, M_{Sun} is solar mass, R_{Sun} is solar radius, Ω is Sun's angular velocity, $\rho = \mu\, m_H N_e$ is the mass density, N_e is electron number density, V_P is the poloidal velocity of the solar wind flow, B_t is the toroidal component of the magnetic field **B** and subscript *eff* indicates wave terms could be present. In the case of q_{eff} we assume the heat flux is field aligned. In a paper by Sittler & Ofman (2006) we made initial attempt to combine our solutions for T_{eff} and q_{eff} within the confines of a 2D MHD model. In Airapetian et al. (2011) they used 3D tomography techniques developed by Kramar *et al.* (2009) for STEREO COR1 3D observations of solar corona reducing it to 2D. These same techniques can be used for our full 3D modeling of the corona and solar wind. For 3D semi-empirical MHD model one will need a more realistic version of the empirical electron density model in Eq. 7.1 such as shown in Eq. 8.7 which will continue to display the desirable asymptotic solutions far from the Sun:

$$N_e(r, \theta, \phi) = N_0 z^2 P_1(z, \theta, \phi) \exp[-\alpha z P_2(z, \theta, \phi)] \tag{8.7}$$

For which now the functions $P_1(z, \theta, \phi)$ and $P_2(z, \theta, \phi)$ with $z = 1/r$ are Legendre Polynomials in co-latitude θ and azimuthal angle ϕ.

8.2. *Set Boundary Conditions*

In order to solve for the above equations certain field line constants and boundary conditions must be established. The constant $\alpha = \rho V/B$ at the equator can be set using the mass flux equation at 1 AU by knowing the solar wind speed $V_{P\infty}$, the electron density $N_e(R_{AU})$ and the radial component of the magnetic field B_r which can all be measured by near Earth spacecraft. The field line equation can be used for $\boldsymbol{B}(r)$ and using the density and velocity variations with latitude using the *Ulysses* plasma observations one can solve for $\alpha(r, \theta)$ for all field lines. This will then allow us to solve for the integral for T_{eff} which is integrated along an open field line to 1 AU. Once this is done, one can the use the equation for q_{eff} to solve for the heat flux for all (r, θ). An example of such 2D maps of flow velocity, effective temperature and effective heat flux are given in Sittler & Guhathakurta (1999, 2002).

9. Summary and Future Work

We have presented our solar eclipse observations for the August 21, 2017 eclipse and the July 2, 2019 eclipse. The seeing was excellent in both cases. Both sets of images have used raw data files which will allow quantitative analysis of these images and convert them into electron density profiles as outlined in Guhathakurta *et al.* (1996) and references therein. For the future we plan to process these images as outlined in this paper and then convert them into 2D maps of the solar wind velocity, effective temperature and effective heat flux for which the 2019 eclipse observations will be used when the Sun is near solar minimum and the 2D axisymmetric assumption is most applicable. Hopefully this effort will be successful and can be compared with other publications based on similar eclipse observations. Within the equatorial regions it will be interesting to see how they compare to the Parker Solar Probe observations.

Even further into the future, using a more general approach as previously discussed, 3D MHD semi-empirical model could be developed but instead of setting our boundary conditions at 1 AU or far from the Sun, one needs to set those constraints near the Sun. A key to this is to use as a local condition to solve for the field-line constant on individual flux tubes with $\alpha(r, \theta, \phi) = \rho V_{||}/B_{||}$ using the local field-aligned components of $\mathbf{V}$ and $\mathbf{B}$. Also, note locally $1/B$ gives the area of a unit flux tube. Once $\alpha(r, \theta, \phi)$ is known then the other equations can be integrated for effective temperature and effective heat flux. These can then be used as constraints on the 3D MHD solutions which will give the 3D magnetic field topology which can then be used for a next iteration of the semi-empirical solution until convergence occurs. A more advanced version of STEREO may be required for 3D solutions of the lower to middle corona as discussed here.

Acknowledgments

References

Airapetian, V., Ofman, L., Sittler, E. C., Jr., & Kramar, M. 2011. Probing the thermodynamics and kinematics of solar coronal streamers, *Astrophys. J.*, 728:67, 1.

Beskeen, P. 2009, http://www.beskeen.com/projects/dsir_serial/dsir_serial.shtml version 2.12, March 2009.

Clark, R. N. 2013, http://www.clarkvision.com/articles/digital.photons.and.qe/, last updated January 4, 2013.

Druckmüller, M. 2009, Phase correlation method for the alignment of total solar eclipse images, *Astrophys. J.*, 706, 1605–1608, doi:10.1088/0004-637X/706/2/1605.

Habbal, S. R., Cooper, J. F., Daw, A., Ding, A., Druckmüller, M., Esser, R., Johnson, J., & Morgan, H. 2011, Exploring the Physics of the corona with total solar eclipse observations, https://arxiv.org/abs/1108.2323 arXiv:1108.2323 [astro-ph.SR].

Guhathakurta, M., Holzer, T. E., & MacQueen, R. M. 1996, The large-scale density structure of the solar corona and the heliospheric current sheet, *Astrophys. J.*, 458, 817–831.

Hulst, H. C. van de, 1950, The electron density of the solar corona, Bull. Astron. Inst. Netherlands, 11, 135–150.

Hulst, H. C. van de, 1953, Chapter 5: The chromosphere and the corona, in *The Sun* (Univ. of Chicago Press).

Kramar, M., Jones, S., Davila, J., Inhester, B., & Mierla, M. 2009, On the tomographic reconstruction of the 3D electron density for the solar corona from STEREO COR1 data, *Solar Physics*, 259, 109–121.

Reddy, S. B. & Chatterji, B. N., 1996, An FFT-Based technique for translation, rotation, and scale-invariant image registration, IEEE Trans. Image Process., 5, 1266–1271.

Schild, R. E., Peterson, D. M., & Oke, J. B. 1971, Effective temperatures of B- and A- Type stars, *Astrophys. J.,* 166, 95.

Sittler, E. C., Jr. & Guhathakurta, M. 1999, Semiempirical two-dimensional magnetohydrodynamic model of the solar corona and interplanetary medium, *Astrophys. J.*, 523, 812–826.

Sittler, E. C., Jr. & Guhathakurta, M. 2002, Erratum: "Semiempirical two-dimensional magnetohydrodynamic model of the solar corona and interplanetary medium" (ApJ, 523, 812 [1999]), *Astrophys. J.*, 564, 1062–1065.

Sittler, E. C., Jr. & Ofman, L. 2006, 2D MHD model of the solar corona and solar wind: Recent results, ILWS Workshop 2006, Goa, February 19–20, 2006.

Sumner, R. 2014, Processing RAW Images in MATLAB, https://rcsumner.net/raw guide/RAWguide.pdf, May 19, 2014.

Woo, R. 2019, Naked eye observations of the 2017 total solar eclipse: a more complete understanding of the white-light corona, *MNRAS* 485, 4122–4127.